Enhancement of biomixing by swimming algal cells in two-dimensional films

Hüseyin Kurtuldu[a], Jeffrey S. Guasto[b], Karl A. Johnson[c], and J. P. Gollub[a,d,1]

[a]Department of Physics, Haverford College, 370 Lancaster Avenue, Haverford, PA 19041; [b]Department of Civil and Environmental Engineering, Massachusetts Institute of Technology, 15 Vassar Street, Cambridge, MA 02139; [c]Department of Biology, Haverford College, 370 Lancaster Avenue, Haverford, PA 19041; and [d]Department of Physics, University of Pennsylvania, 209 South 33rd Street, Philadelphia, PA 19104

Contributed by J. P. Gollub, May 4, 2011 (sent for review March 29, 2011)

Fluid mixing in active suspensions of microorganisms is important to ecological phenomena and presents a fascinating stochastic process. We investigate the mixing produced by swimming unicellular algal cells (*Chlamydomonas*) in quasi-two-dimensional liquid films by simultaneously tracking the motion of the cells and that of microscopic passive tracer particles advected by the fluid. The reduced spatial dimension of the system leads to long-range flows and a surprisingly strong dependence of tracer transport on the concentration of swimmers, which is explored over a wide range. The mean square displacements are well described by a stochastic Langevin model, which is used to parameterize the mixing. The effective diffusion coefficient D grows rapidly with the swimmer concentration Φ as $D \sim \Phi^{3/2}$, as a result of the increasing frequency of tracer-swimmer interactions and the long-range hydrodynamic disturbances created by the swimmers. Conditional sampling of the tracer data based on the instantaneous swimmer position shows that the rapid growth of the diffusivity enhancement with concentration must be due to particle interactions with multiple swimmers simultaneously. Finally, the anomalous probability distributions of tracer displacements become Gaussian at high concentration, but manifest strong power-law tails at low concentration, while the tracer displacements always grow diffusively in time.

biofluid dynamics | low Reynolds number | flagella

Biomixing is the enhancement of material transport by motile organisms in nature. It has been suggested that macroscopic organisms at high Reynolds number may contribute significantly to biogenic mixing at global scales, for example in the ocean, via turbulent wake mixing or the dragging of fluid during swimming (1). Microorganisms, on the other hand, experience a vastly different environment dominated by viscous forces at low Reynolds number that make mixing difficult. While estimates of their relative contribution to global mixing are uncertain (2, 3), microorganisms can have a substantial impact on local mixing at cellular scales. For example, the fluid flows produced by the beating flagella of microorganisms play an important role in mediating diffusion-limited nutrient uptake of solutes by single cells (4) and colonial multicellular organisms (5). These flows also affect particle capture in suspensions of swimmers that engulf particles (6). Microfluidic devices can exploit these effects to enhance mixing in microfluidic channels (7) and to control or direct material transport (8, 9) using either cell cultures or artificial swimmers (10).

Mixing by microswimmers is best described statistically (11), and has been studied in several previous investigations. Wu and Libchaber (12) introduced the concept of an effective "thermal bath" to describe the enhanced diffusion of large particles caused by swarming *Escherichia coli* bacteria, as an analog to Brownian motion resulting from molecular collisions (13). Leptos et al. (14) demonstrated that in dilute suspensions of the green alga *Chlamydomonas reinhardtii* the probability distribution functions (PDFs) of tracer displacements (velocities) deviate from Gaussianity, manifesting strong exponential tails in three dimensions (14), due apparently to large advective displacements caused by the flow fields of passing swimmers (15, 16). Similar anomalous statistical features appear in a variety of other systems as well (17–19). A number of recent numerical (20–22) and experimental (10) studies have helped to elucidate these phenomena; however, tracer statistics in the transition regime from dilute to concentrated cell distributions are still not well understood. In a significant experimental development, Rushkin et al. (23) showed that flow field velocity PDFs in suspensions of the multicellular colonial green alga *Volvox carteri* converge to Gaussians with increasing organism concentration as a result of random superposition of their advective fields.

In this paper, we investigate the statistics of microscale fluid mixing in a quasi-two-dimensional system due to an active suspension of unicellular swimmers (*C. reinhardtii*). Similar confinement can also occur in biofilms and in cellular transport near free surfaces (24, 25), as well as in thin, mucous layers over ciliated epithelia, such as line the human trachea (26). In our experiments, passive tracer particles are tracked simultaneously along with motile cells in a thin fluid film. We find that the enhanced tracer diffusivity grows much faster with cell concentration than occurs in three dimensions. Small swimmer concentrations yield extended power-law tails in the probability distributions of tracer displacement, due to the long-range hydrodynamic disturbances created by swimmers in quasi-two-dimensional environments (15). We show that the distributions become Gaussian at high cell volume fraction ($\Phi \approx 7\%$). This behavior results from the simultaneous perturbations of individual tracers by the overlapping velocity fields of multiple swimmers; we also explore the role of interactions between swimmers. Finally, the statistical properties of the enhanced transport are studied conditionally as a function of a tracer's proximity to the nearest swimmer to give further insight into the statistics of biomixing.

Results

Tracer Dynamics. *C. reinhardtii* is a single-celled biflagellated green alga with a body diameter $d \approx 10$ μm and two anterior flagella almost equal in length to the body diameter (27). Each cell swims by beating its flagella at 50–60 Hz in a breaststroke motion, which propels the organism at a mean speed of $U_0 \approx 100$ μm/s (15).

A suspension of cells and microscopic polystyrene tracer particles is stretched into a thin film and observed using video microscopy, as explained in *Materials and Methods*. A sample image showing detected cells and tracer particles is shown in Fig. 1*A*. The cells are randomly distributed throughout the area of the freely suspended thin film (thickness $h = 15 \pm 5$ μm), though of course their separations vary. The nearest neighbors are Poisson distributed with a mean spacing $\langle s \rangle$ that varies with concentration Φ (measured cell volume per unit volume of suspension) as $\langle s \rangle \sim \Phi^{-0.47}$. Our measurements (Fig. 1*B*) are in

Author contributions: J.P.G. designed research; H.K., J.S.G., K.A.J., and J.P.G. performed research; K.A.J. contributed new reagents/analytic tools; H.K. analyzed data; and H.K., J.S.G., K.A.J., and J.P.G. wrote the paper.

The authors declare no conflict of interest.

[1]To whom correspondence should be addressed. E-mail: jgollub@haverford.edu.

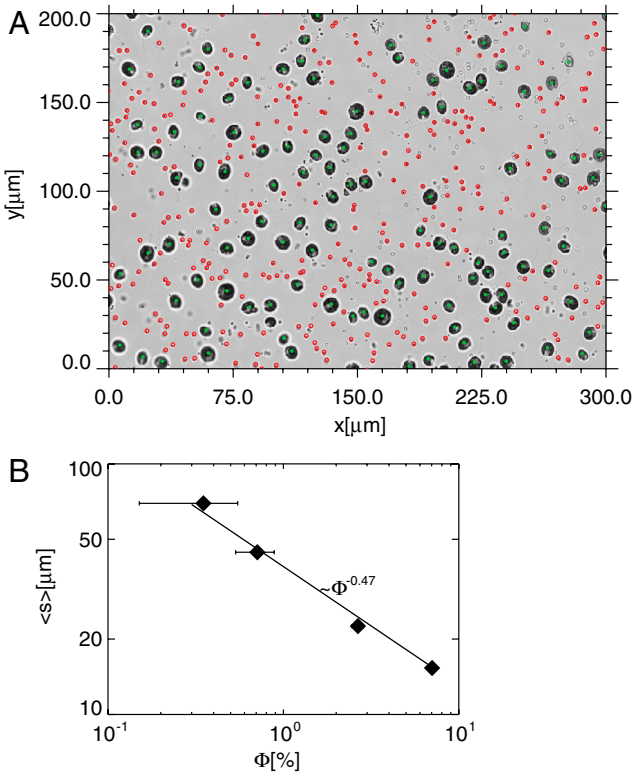

Fig. 1. (*A*) Sample image of a typical field for $\Phi = 7.0\%$ showing the identified $d \approx 10$ μm diameter swimming cells (green) and 1 μm passive tracers (red) in a ~15 μm thin film. Cells and tracers are tracked in successive frames and formed into trajectories from the video data. The cells move about 100 μm on average in 1 s and perturb the tracer particles as they swim. (*B*) The measured mean nearest-neighbor distance $\langle s \rangle$ for the swimmers decreases with increasing cell volume fraction Φ, as expected. The solid line represents a power-law fit $\langle s \rangle = 0.44 d\Phi^{-0.47}$, which agrees with the expected result for Poisson distributed nearest-neighbors and a layer thickness comparable to the cell diameter.

agreement with the expected result (28) $\langle s \rangle = \frac{\sqrt{\pi}}{4} d\Phi^{-1/2}$ for a liquid film of thickness equal to the cell diameter. For thicker layers, the coefficient would be smaller.

As the swimmers move within the film, they randomly perturb the tracer particles. The rate and amplitude of tracer particle fluctuation increase with the volume fraction Φ of swimmers. The trajectories of three sample particles along one axis of motion are shown in Fig. 2 at different swimmer volume fractions. At

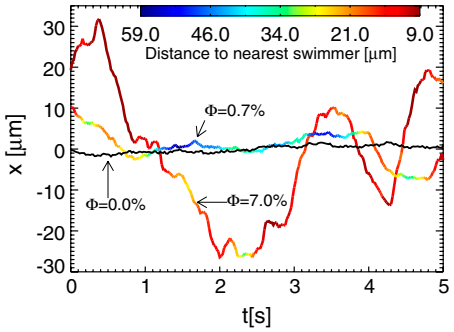

Fig. 2. Trajectories of sample tracer particles along one axis over 5 s, as a result of random, advective displacements by nearby swimming cells for three different volume fractions Φ. The amplitude of the position fluctuations becomes larger with increasing swimmer concentration. The color of the trajectory represents the particle's distance from the nearest swimmer for $\Phi = 7.0\%$ and 0.7%. The black curve corresponds to $\Phi = 0.0\%$, measured in the absence of swimmers where only Brownian motion is acting.

$\Phi = 0\%$ (i.e., no swimmers), low-level random noise is due solely to Brownian, thermal fluctuations. As the swimmer concentration increases ($\Phi = 0.7\%$), the amplitude of the random background fluctuations increases as well. Intermittent large amplitude displacements are also observed that correlate with the nearby passage of a single swimmer. This behavior can be observed in Fig. 2, where the trajectory color indicates the distance to the nearest swimmer. The motion results from the advective displacement associated with the flow field disturbances of passing swimmers, and appears random over long times (or equivalently when averaged over an ensemble). At the highest swimmer concentration ($\Phi = 7.0\%$), the intermittency between the kicks is no longer apparent, and the particle trajectories appear as large amplitude white noise, substantially larger than Brownian motion alone could produce.

Ensemble Statistics and Departures from Gaussianity. The PDFs of tracer displacements $P(\Delta x; \Delta t)$ (14) are measured for a wide range of volume fractions and different time intervals Δt (Fig. 3) in order to investigate the statistics of the fluctuations. In the absence of swimmers (i.e., $\Phi = 0\%$), the displacement PDF is Gaussian to good precision (e.g., at $\Delta t = 0.04$ s), as one would expect for Brownian motion (Fig. 3*A*). At small $\Phi \leq 0.7\%$, swimmers give strong perturbations to a small fraction of tracers in their immediate vicinity, inducing displacements that are much larger than the Brownian fluctuations. Over the entire ensemble of tracer particles, these low probability, high amplitude events contribute to the tails of the displacement distribution (Fig. 3*A*), while the majority of the tracers, far from any swimmer, experience little advection. The tails become weaker with increasing Δt as seen in Fig. 3*B* for $\Phi = 0.3\%$. At short Δt the tails have a power-law form, decaying approximately as $P(\Delta x) \sim \Delta x^{-4}$, which is significantly different from the exponential form found in unbounded, three-dimensional (3D) suspensions of *Chlamydomonas* (14).

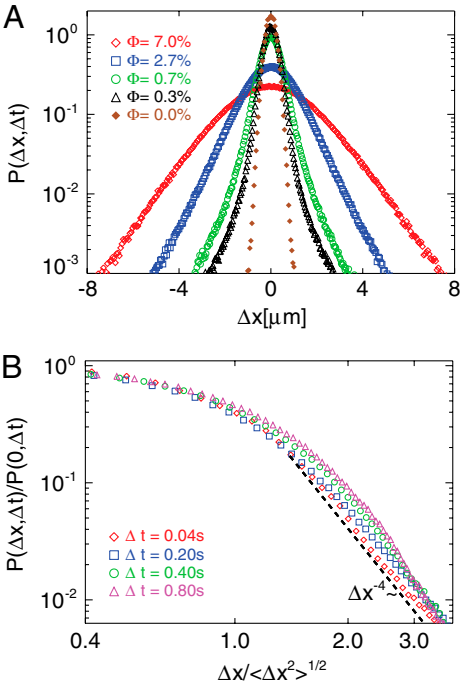

Fig. 3. (*A*) PDFs of tracer displacements during a fixed short time interval ($\Delta t = 0.04$ s) and at various volume fractions Φ. Heavy power-law tails are apparent for $\Phi \leq 0.7\%$. (*B*) Normalized and rescaled PDFs at increasing Δt and fixed concentration ($\Phi = 0.3\%$). At short times the tails vary as $P(\Delta x) \sim \Delta x^{-4}$ (dashed line), and become progressively weaker with increasing Δt.

A possible explanation for this contrasting behavior of 2D and 3D systems may be deduced from the nature of the swimmer's velocity field in a system with reduced spatial dimension. In 3D, the fluid velocity around a swimming microorganism that is not acted on by any external force typically decays as the inverse square of the distance ($u \sim r^{-2}$) from the organism (16) due to the dominance of the force dipole (stresslet) (29). In a thin film, on the other hand, the force dipole's velocity field is shown to scale as $u \sim r^{-1}$ (15). The consequences of this slower falloff of the induced velocity may be seen in recent experiments on negatively buoyant *Volvox carteri*, a multicellular alga comprised of thousands of *Chlamydomonas*-like cells, which show a $u \sim r^{-1}$ decay due to the dominance of the monopole (Stokeslet) singularity for these dense microorganisms in the external gravitational field (23). The long-ranged swimmer velocity field gives rise to tails in the short time displacement distribution of the surrounding fluid, varying approximately as $P \sim \Delta x^{-4}$. Although the cause of the long-ranged velocity field is different here (reduced dimensionality rather than density mismatch), the same arguments can be applied.

Interestingly, the extended tails disappear at higher cell concentration ($\Phi = 7.0\%$) (Fig. 3*A*), giving rise to a significantly broadened PDF that approaches a Gaussian. In order to investigate the convergence to a normal distribution with increasing Φ and Δt, we use the measure of excess kurtosis γ_2, which characterizes the departure from Gaussianity. The excess kurtosis is defined as $\gamma_2 = \mu_4/\mu_2^2 - 3$, where μ_k is the kth moment of the displacement distribution and thus, $\gamma_2 = 0$ for a Gaussian. As shown in Fig. 4*A*, the absence of swimmers yields $\gamma_2 \approx 0$, as expected for a purely Brownian random walk. For a low swimmer concentration ($\Phi \leq 0.7\%$), the strong power-law tails give $\gamma_2 > 0$, especially at short Δt [Fig. 4*A* (inset)]. As the number of random kicks increases with Δt, we find that γ_2 decays, converging toward Gaussianity asymptotically in the limit of our experimental observation time. At even higher swimmer densities ($\Phi \geq 2.7\%$), the displacement PDFs rapidly converge to Gaussian ($\gamma_2 = 0$) for relatively short Δt.

Fig. 4*B* shows the PDFs at a fixed interval ($\Delta t = 0.2$ s) and demonstrates the convergence to a Gaussian distribution with increasing concentration. This observation is consistent with a recent study (30), where tracer diffusion was investigated both analytically and numerically for flow fields that decay as $u \sim r^{-n}$ in the vicinity of a swimmer. That study predicted that for $n = 1$ as in our work (15), the velocity (and displacement) PDFs of tracers should converge to a Gaussian distribution, while by contrast the distributions should exhibit strong non-Gaussianity for $n \geq 2$, even at large Φ, as was found previously in 3D *Chlamydomonas* suspensions (14).

Enhanced Transport. The broad probability distributions whose widths grow with Δt indicate significantly enhanced transport. For each Φ we measure the mean square displacements of particles $\langle \Delta x^2 \rangle$, where $\langle\rangle$ indicates an ensemble average over thousands of particles. We observe diffusive scaling $\langle \Delta x^2 \rangle \sim \Delta t^{\alpha}$, with $\alpha \approx 1.0$, for $\Phi = 0.0\%$ at all Δt (Fig. 5*A*). For $\Phi > 0$, this diffusive regime begins to appear at subsequently longer Δt as Φ increases, with an anomalous transport ($1.5 < \alpha < 2.0$) at shorter Δt. This behavior has been seen in bacterial suspensions (12), but not in an algal suspension (14).

The time evolution of the position of a particle exhibiting Brownian-like motion, due to a combination of thermal motion and swimmer collisions, can be described by a Langevin model and parameterized by an effective diffusivity D (12, 31). A solution to such a stochastic model in one dimension can be written as

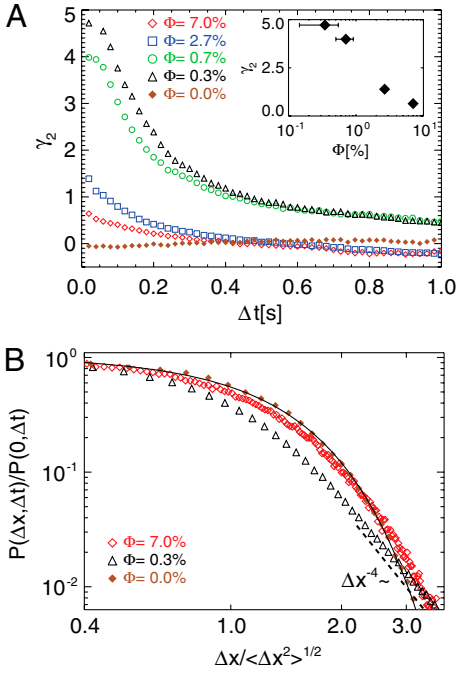

Fig. 4. (*A*) The excess kurtosis γ_2 computed from the displacement PDFs as a function of time interval Δt for different values of volume fraction Φ. The value $\gamma_2 = 0$ corresponds to a Gaussian distribution. In the inset, γ_2 is shown for different values of Φ at $\Delta t = 0.02$ s. (*B*) Normalized and rescaled PDFs for positive Δx are shown for three different volume fractions Φ at $\Delta t = 0.2$ s, demonstrating convergence to a Gaussian at large Φ. The solid line is a nonlinear least squares Gaussian fit to the Brownian data ($\Phi = 0.0\%$), and the dashed line shows the consistency of the tail with Δx^{-4} for the dilute case.

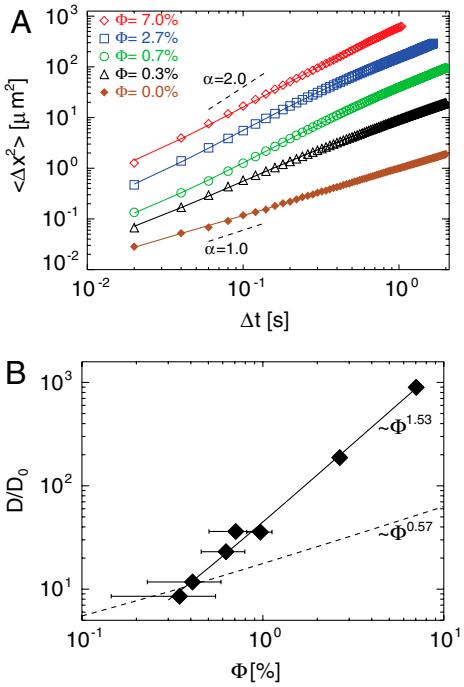

Fig. 5. (*A*) Mean square tracer displacements for various swimmer volume fractions Φ, where the solid lines are the Langevin functional fits to Eq. **1**. Two dashed lines are drawn to show the slopes $\alpha = 1.0$ and $\alpha = 2.0$. (*B*) The effective diffusion coefficient D, normalized by the measured Brownian diffusivity D_0, is shown as a function of Φ. The horizontal error bars represent the uncertainty in Φ; the vertical error bars are too small to be seen. The solid line represents a power-law fit $D \sim \Phi^{1.53}$, and the dashed line $D \sim \Phi^{0.57}$ is the diffusivity scaling in the dilute limit, estimated in the section on conditional sampling. The rapid growth of D with Φ is evident.

$$\langle \Delta x^2 \rangle = 2D[\Delta t + \tau(e^{-(\Delta t/\tau)} - 1)], \quad [1]$$

where τ defines a characteristic correlation time (32). For $\Delta t \gg \tau$, the particle displacements are diffusive ($\alpha = 1$) with $\langle \Delta x^2 \rangle \simeq 2D\Delta t$. For Brownian motion alone, $D = k_b T/6\pi\eta a$ from the Einstein-Smolukowski relation, where k_b, T, η, and a are Boltzmann's constant, the absolute temperature, the dynamic viscosity, and the particle radius, respectively. In experiments performed at room temperature, we expect $D = 0.49\ \mu m^2/s$ for 1 μm diameter particles.

In order to estimate D in the presence of swimmers, we fit the mean square displacement (MSD) data given in Fig. 5*A* to Eq. **1** using nonlinear least squares. For the case of no swimmers, we obtain $D = 0.48\ \mu m^2/s$ consistent with the theoretical estimate. As delineated in Fig. 5*B*, D has a nonlinear dependence on the swimmer volume fraction; it grows like a power-law with $D \sim \Phi^{3/2}$. Even for the most dilute swimmer suspension ($\Phi = 0.3\%$), the diffusion is enhanced by almost a factor of 10 compared to Brownian diffusion alone. Strikingly, the reduced dimensionality leads to a major enhancement of diffusion. At $\Phi = 2.7\%$ for example, D/D_0 is about 10.5 in three dimensions (14) compared to $D/D_0 \simeq 190$ in two dimensions.

Previously, it was predicted based on simulations that unicellular swimmers with posterior locomotor appendages ("pushers," e.g., *Escherichia coli*) would increase the fluid transport by a far greater factor than cells with anterior flagella ("pullers") in 3D suspensions (33, 34). The basic cause was the presence of collective behavior (35), i.e., large scale vortices and jets, for the bacteria. On the other hand, our experimental results suggest that the swimming style of active particles may not play a major role in the degree of transport enhancement for dilute and semidilute swimmer suspensions. We find that the enhancement factors at comparable volume fractions are similar for *Chlamydomonas* and *E. coli*, despite the apparent absence of collective behavior for the *Chlamydomonas*. For example, we find $D/D_0 \simeq 900$ at $\Phi = 7.0\%$ ($\simeq 1.3 \times 10^8$ cells/mL) for a puller, only a factor of 2 smaller than $D/D_0 \simeq 2{,}200$ at $\Phi \simeq 10\%$ ($\simeq 5.4 \times 10^{10}$ cells/mL) for *E. coli* (12). However, direct comparisons between species are difficult to make with confidence.

Conditional Sampling and the Concentration Dependence of Diffusivity. Based on our knowledge of the instantaneous trajectories of *both* the tracer particles and the swimmers, we can conditionally sample tracer statistics based on their proximity to a cell. For example, we determine the diffusivity enhancement for those particles that are located within a radial distance r_w from the center of the nearest swimmer during a time interval Δt. The mean square displacement analysis and Langevin fit are then repeated to obtain D for a variety of r_w and for each swimmer volume fraction Φ.

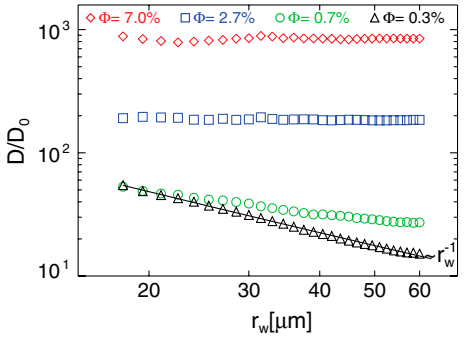

Fig. 6. Conditional sampling analysis showing the effective diffusivity D, normalized by the Brownian value, for only those tracer particles that are within a given distance r_w of the nearest swimmer. As the swimmer concentration increases, D/D_0 becomes independent of r_w.

The results of this analysis are shown in Fig. 6. Before discussing the results, we note that for sufficiently dilute suspensions (e.g., $\Phi = 0.3\%$), the advective kicks imparted to a tracer particles are solely due to a single swimmer at any given time. In this range, varying r_w is analogus to varying Φ. We estimate the region where this "dilute limit" assumption is valid by determining the distance δ at which advective disturbances are comparable to Brownian noise (i.e., Péclet number ~1): $u(\delta)\Delta t = \sqrt{4D\Delta t}$, where Δt is the time between successive video frames, and $u(r)$ is the radially decaying velocity magnitude, measured previously for freely swimming *Chlamydomonas* cells (15). We estimate that the range of the advective disturbances is $\delta \approx 22$ μm from a swimmer. For inter-swimmer separations $\langle s \rangle$ (i.e., the average distance between the closest pairs of swimmers) significantly larger than this distance (e.g., $\langle s \rangle \geq 2\delta$), tracers should be influenced by only a single swimmer at a time.

The conditionally sampled diffusivity enhancement D/D_0 decays as $D \sim r_w^{-1}$ in this dilute regime. Equivalently, in terms of the volume fraction $\Phi \simeq (d/2r_w)^2$, the implied enhancement in the dilute limit varies as $D/D_0 \sim \Phi^{1/2}$. Comparing this estimate to the measured scaling of $D/D_0 \sim \Phi^{3/2}$ shown in Fig. 5*B* demonstrates that the stronger enhancement observed in the film must be due to particle interactions with multiple swimmers simultaneously.

In the concentrated regime, on the other hand, where tracers are influenced by many swimmers, Fig. 6 shows that the enhancement factor becomes independent of r_w but has a strongly nonlinear dependence on Φ.

The Possible Effect of Swimmer Interactions on Transport. In addition to the overlapping advective velocity fields induced by multiple swimmers, swimmer-swimmer interactions may also play a role in the enhancement of diffusion (34). The nature of swimmer-swimmer interactions is yet to be determined experimentally, i.e., whether the interactions are through mechanical contact or hydrodynamic scattering. However, it is known that two nearby swimmers can modify each other's intrinsic swimming paths (36–38). Here, we demonstrate quantitatively from the shapes of the swimmer trajectories that the swimmers turn more frequently as the inter-swimmer distance $\langle s \rangle$ decreases. We do so by measuring the swimming path curvature $\kappa = |\nabla \cdot \mathbf{n}|/2$, where $\mathbf{n}$ is the unit vector normal to the direction of movement (39). Fig. 7 shows the PDFs of path curvature at a given Φ, and the mean curvature [Fig. 7 (inset)] for increasing $\Phi \sim \langle s \rangle^{-2}$. The broadening of the distribution indicates that the swimmers follow more highly deflected trajectories when the swimmer-swimmer encounter rate increases. To what extent swimmer interactions affect the diffusivity is still unknown experimentally, but could be responsible for the strong concentration dependence, and is an important topic for future work.

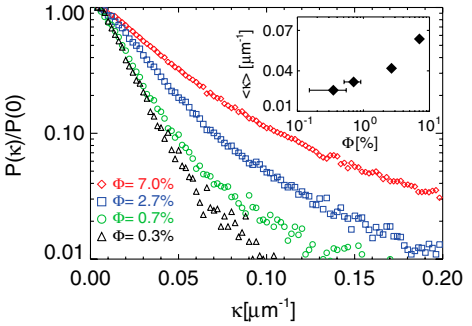

Fig. 7. Probability distribution of the curvature κ of cell trajectories at different swimmer volume fractions Φ. The inset shows the growth of the mean curvature $\langle \kappa \rangle$ for increasing Φ.

Conclusion

We have shown that reduced spatial dimensionality dramatically enhances the mixing induced by suspensions of swimming algal cells. The enhanced diffusivity grows as $D/D_0 \sim \Phi^{3/2}$, which is significantly faster than in three dimensions, due to the long-range hydrodynamic disturbances of the swimmers ($u \sim r^{-1}$) as well as an increased frequency of interaction with the passive tracers.

Some insight into the origin of the enhancement can be obtained by looking separately at the mean square tracer speed $\langle u^2 \rangle$, and the characteristic time τ in the Langevin fit. The enhanced diffusion could then be related via $D \sim \langle u^2 \rangle \tau$ (31). We find that $\langle u^2 \rangle$ grows linearly with concentration, while τ grows approximately as $\Phi^{1/2}$, thus accounting for the overall variation $\Phi^{3/2}$. We also note that the predicted enhancement of tracer diffusion due to the film geometry alone (40) is not significant (41), as the particles are about 15 times smaller than the film thickness.

We also found that the statistics of the induced tracer displacement fluctuations exhibit highly anomalous behavior of the probability distributions. The distributions show power-law tails in the dilute regime owing to the intermittent agitation by passing swimmers. As the number density of swimmers increases, the intermittency gives way to large amplitude random forcing and a return to Gaussianity due to the simultaneous influence of multiple swimmers on any given tracer particle.

Materials and Methods

Wild-type *C. reinhardtii* (cc1690) are first grown on culture in minimal media (M1) and synchronized on a 12 h bright/dark light cycle to optimize motility and cell size uniformity (27). Higher concentrations are achieved by concentrating cells through centrifugation and resuspension. Following the procedures of Guasto et al. (15), an aliquot of the cell culture is mixed with 1 μm diameter polystyrene microsphere tracers (Thermo Scientific) and a trace amount of surfactant (Tween 20, 0.03% v/v) is added to the mixture to lower the surface tension of the cell suspension. A 2 μL droplet of the suspension is stretched on an adjustable wire-frame device to obtain a stable thin film with a thickness of $h = 15 \pm 5$ μm (similar to ref. 15). Visualization is performed using an upright bright field microscope with a 40× magnification objective, and a high speed camera (Cooke pco.1,200 hs) is used to capture the motion of the cells and the tracers in the film at 50 fps for 2,800 frames. The confinement of the cells in a quasi-two-dimensional environment provides in-focus observation of all cells through the film depth and enables the simultaneous tracking of both cells and tracers for relatively long times ($\lesssim$5 s). Image processing is performed in IDL, where the cells and tracers are segmented from the images and identified from one another based on size (see Fig. 1*A*). An efficient predictive particle tracking algorithm (42) is implemented to track the cells and tracers from the time series of images. The volume fraction Φ is determined by the number of cells averaged over time in the field of view. At a given Φ, reasonable sample sizes are used for analysis; for example, we choose the range of r_w shown in Fig. 6 that gives accurate statistics for the full range of Φ.

ACKNOWLEDGMENTS. This work was supported by the National Science Foundation under Grant No. NSF DMR-0803153.

1. Katija K, Dabiri JO (2009) A viscosity-enhanced mechanism for biogenic ocean mixing. *Science* 460:624–626.
2. Visser AW (2007) Biomixing of the oceans? *Science* 316:838–839.
3. Kunze E, Dower JF, Dewey R, D'Asaro EA (2007) Mixing it up with Krill. *Science* 318:1239.
4. Tam D, Hosoi AE (2011) Optimal feeding and swimming gaits of biflagellated organisms. *Proc Natl Acad Sci USA* 108:1001–1006.
5. Short MB, et al. (2006) Flows driven by flagella of multicellular organisms enhance long-range molecular transport. *Proc Natl Acad Sci USA* 103:8315–8319.
6. Humphries S (2009) Filter feeders and plankton increase particle encounter rates through flow regime control. *Proc Natl Acad Sci USA* 106:7882–7887.
7. Kim MJ, Breuer KS (2004) Enhanced diffusion due to motile bacteria. *Phys Fluids* 16:78–81.
8. Kim MJ, Breuer KS (2007) Controlled mixing in microfluidic systems using bacterial chemotaxis. *Anal Chem* 79:955–959.
9. Sokolov A, Apodac MM, Grzybowski BA, Aranson IS (2010) Swimming bacteria power microscopic gears. *Proc Natl Acad Sci USA* 107:969–974.
10. Mino G, et al. (2011) Enhanced diffusion due to active swimmers at a solid surface. *Phys Rev Lett* 106:048102.
11. Saintillan D, Shelley MJ (2008) Instabilities, pattern formation and mixing in active suspensions. *Phys Fluids* 20:123304.
12. Wu X-L, Libchaber A (2000) Particle diffusion in a quasi-two-dimensional bacterial bath. *Phys Rev Lett* 84:3017–3020.
13. Brown R (1828) A brief account of microscopical observations made in the months of June, July and August, 1827, on the particles contained in the pollen of plants; and on the general existence of active molecules in organic and inorganic bodies. *Philos Mag* 4:161–173.
14. Leptos KC, Guasto JS, Gollub JP, Pesci AI, Goldstein RE (2009) Dynamics of enhanced tracer diffusion in suspension of swimming Eukaryotic microorganisms. *Phys Rev Lett* 103:1981103.
15. Guasto JS, Johnson KA, Gollub JP (2010) Oscillatory flows induced by microorganisms swimming in two dimensions. *Phys Rev Lett* 105:168102.
16. Drescher K, Goldstein RE, Michel N, Polin M, Tuval I (2010) Direct measurement of the flow field around swimming microorganisms. *Phys Rev Lett* 105:168101.
17. Wang B, Anthony SM, Bae SC, Granick S (2009) Anomalous yet Brownian. *Proc Natl Acad Sci USA* 106:15160–15164.
18. Chaudhuri P, Berthier L, Kob W (2007) Universal nature of particle displacements close to glass and jamming transitions. *Phys Rev Lett* 99:060604.
19. Nicolaides C, Cueto-Felgueroso L, Juanes R (2010) Anomalous physical transport in complex networks. *Phys Rev E* 82:055101(R).
20. Lin Z, Thiffeault J-L, Childress S (2011) Stirring by squirmers. *J Fluid Mech* 669:167–177.
21. Ishikawa T, Locsei JT, Pedley TJ (2010) Fluid particle diffusion in a semidilute suspension of model micro-organisms. *Phys Rev E* 82:021408.
22. Dunkel J, Putz VB, Zaid IM, Yeomans JM (2010) Swimmer-tracer scattering at low Reynolds number. *Soft Matter* 6:4268–4276.
23. Rushkin I, Kantsler V, Goldstein RE (2010) Fluid velocity fluctuations in a suspension of swimming Protists. *Phys Rev Lett* 105:188101.
24. Oliver JK, Willis BL (1987) Coral-spawn slicks in the great barrier reef: preliminary observations. *Mar Biol* 94:521–529.
25. Blanchard DC (1989) The ejection of drops from the sea and their enrichment with bacteria and other materials: a review. *Estuaries* 12:127–137.
26. Matsui H, Randell SH, Peretti SW, Davis CW, Boucher RC (1998) Coordinated clearance of periciliary liquid and mucus from airway surfaces. *J Clin Invest* 102:1125–1131.
27. Harris EH (1999) *The Chlamydomonas sourcebook* (Academic Press, Oxford).
28. Selvin S (2004) *Statistical Analysis of Epidemiologic Data* (Oxford University Press, New York).
29. Lauga E, Powers TR (2009) The hydrodynamics of swimming microorganisms. *Rep Prog Phys* 72:096601.
30. Zaid IM, Dunkel J, Yeomans JM (2011) Lévy fluctuations and mixing in dilute suspensions of algae and bacteria. *J R Soc Interface*, 10.1098/rsif.2010.0545.
31. Darnton N, Turner L, Breuer K, Berg HC (2004) Moving fluid with bacterial carpets. *Biophys J* 86:1863–1870.
32. Amit DJ, Verbin Y (1999) *Statistical Physics: An Introductory Course* (World Scientific, Singapore).
33. Saintillan D, Shelley MJ (2008) Instabilities and pattern formation in active particle suspensions: kinetic theory and continuum simulations. *Phys Rev Lett* 100:178103.
34. Underhill PT, Hernandez-Ortiz JP, Graham MD (2008) Diffusion and spatial correlations in suspensions of swimming particles. *Phys Rev Lett* 100:248101.
35. Zhang HP, Be'er A, Smith RS, Florin EL, Swinney HL (2009) Swarming dynamics in bacterial colonies. *Europhys Lett* 87:48011.
36. Ishikawa T, Hota M (2006) Interaction of two swimming Paramecia. *J Exp Biol* 209:4452–4463.
37. Ishikawa T, Sekiya G, Imai Y, Yamaguchi T (2007) Hydrodynamic interactions between two swimming bacteria. *Biophys J* 93:2217–2225.
38. Pooley CM, Alexander GP, Yeomans JM (2007) Hydrodynamic interaction between two swimmers at low Reynolds number. *Phys Rev Lett* 99:228103.
39. Ouellette NT, Gollub JP (2007) Curvature fields, topology, and the dynamics of spatiotemporal chaos. *Phys Rev Lett* 99:194502.
40. Cheung C, Hwang YH, Wu X-L, Choi HJ (1996) Diffusion of particles in free-standing liquid films. *Phys Rev Lett* 76:2531–2534.
41. Prasad V, Weeks ER (2009) Two-dimensional to three-dimensional transition in soap films demonstrated by microrheology. *Phys Rev Lett* 102:178302.
42. Ouellette NT, Xu H, Bodenschatz E (2006) A quantitative study of three-dimensional Lagrangian particle tracking algorithms. *Exp Fluids* 40:301–313.